ISSN 1024-8560, Atmospheric and Oceanic Optics, 2024, Vol. 37, No. 3, pp. 352–356.

REMOTE SENSING OF ATMOSPHERE, HYDROSPHERE, AND UNDERLYING SURFACE

Effects of Strong Convection in Summer on Atmospheric Characteristics Derived from GNSS Monitoring Data

O. G. Khutorova[a, *], **M. V. Maslova**[a, **], **and V. E. Khutorov**[a, ***]
[a] *Kazan Federal University, Kazan, 420008 Russia*
**e-mail: Olga.Khutorova@kpfu.ru*
***e-mail: maryamaslova1861@mail.ru*
****e-mail: pri870@yandex.ru*
Received July 20, 2023; revised September 25, 2023; accepted September 26, 2023

Abstract—The paper solves the problem of deriving the relationship between the variability of statistical characteristics of atmospheric parameters measured by GNSS receivers and the characteristics of convective processes based on monitoring data near the Kazan city for 2013–2021. The GNSS monitoring results are compared with the convective indices, which are physical and statistical parameters of instability, calculated from ERA5 reanalysis: upward vertical velocity, vortex generation parameter, and WMAXSHEAR. Statistical characteristics of the horizontal gradient of the zenith tropospheric delay are shown to significantly change under conditions of deep convection. The results of the work can be used to develop a technique for sub-satellite monitoring of convective processes in the tasks of operational forecasting of severe weather phenomena.

Keywords: global navigation satellite system, tropospheric monitoring, atmospheric convection, tropospheric zenith delay, gradient parameter

DOI: 10.1134/S1024856024700520

INTRODUCTION

The number of dangerous weather phenomena, such as storm winds, heavy rainfall, and severe thunderstorms associated with mesoscale convective processes has been increasing in recent years [1]. Satellite data, which are used to estimate the integrated water vapor as an indicator of the convection intensity, do not always satisfy the requirement of immediacy. For example, work [2] shows that low sampling frequency limits the applicability of MODIS data for diagnosing conditions for the occurrence of strong squalls and tornadoes. In addition, water vapor fields are strongly spatially variable [3]. In this regard, tropospheric sounding using global navigation satellite systems (GNSS) can be a promising technique for subsatellite monitoring of mesoscale processes.

The purpose of the work is to identify deep convection from tropospheric GNSS monitoring data.

MATERIALS AND METHODS

GNSS provides sounding in both the ionosphere and the troposphere. The main characteristic of the neutral non-ionized atmosphere is the zenith tropospheric delay of satellite radio signals (ZTD), which is calculated from the measured slant tropospheric delay (STD). ZTD depends on meteorological parameters and can be calculated as the integral

$$\mathrm{ZTD} = \int_{\text{detector}}^{\text{satellite}} N \times 10^{-6} ds, \qquad (1)$$

where ds is the element of an integration path; $N = n^{-1}$, n is the refractive index of radio waves along a vertical signal propagation path.

The delay is, in fact, an extra phase path of a radio signal relative to the path in a vacuum; therefore, it is measured in units of length, usually millimeters. ZTD consists of hydrostatic (ZHD) and wet (ZWD) components. The refractive index of air can be divided into two components: hydrostatic, which depends on the air density, and moist, which depends on the partial water vapor pressure.

The main contributor to ZTD is ZHD (~2300 mm), which is stable and can be accurately simulated based on the known values of meteorological parameters on the Earth's surface [4]. ZWD is determined by the partial water vapor pressure in an atmospheric column. Integrating over height, we derive a relationship with the integrated water vapor (IWV), which is usually measured in kg/m^2 or millimeters of precipitable water [5].

Horizontal gradient parameters, which characterize the heterogeneous structure of the troposphere, are introduced into the equation for estimating ZTD from satellite measurements. For further calculations, a Taylor series expansion is applied and first-order terms are taken into account. The resulted equation describes STD accounting the horizontal heterogeneity of the troposphere [6]:

$$\mathrm{STD}^i(t, A^i, z^i) = \mathrm{ZTD}^i(t)m(z^i) + {}^n\mathrm{ZTD}(t)\frac{\partial m}{\partial z}\cos(A^i) + {}^e\mathrm{ZTD}(t)\frac{\partial m}{\partial z}\sin(A^i), \quad (2)$$

where ^{n}ZTD is the meridional gradient parameter at an observation station; ^{e}ZTD is the zonal gradient parameter; A^i is the azimuth direction to the satellite; i is the satellite number; m is the mapping function; z is the zenith angle of the signal path from a satellite to a detector; t is the current time.

Modern studies witness a connection between the inhomogeneous structure of the troposphere and horizontal gradient parameters. According to [7, 8] both zonal and meridional tropospheric gradient parameters of ZTD well agree with mesoscale numerical simulation results and radiometric observations.

The high temporal and spatial resolution of GNSS observations makes it possible to study convective processes. As a rule, variations in IWV intensify before showers [9]. Typical configurations of mesoscale convective cells are shown in the fields of horizontal gradients of IWV [10]. A dense network of GNSS stations made it possible to track the trajectory of the derecho in Poland, the fields of gradient parameters and water vapor showed mesoscale structures observed with microwave radiometer and weather radar [11]. A network of GPS stations was used in Texas to monitor and track the Harvey Hurricane. ZWD and tropospheric gradients correlate with water vapor gradients before and after a hurricane and with wind and pressure gradients only after a hurricane [12].

GNSS sounding enables detecting a variety of mesoscale processes: daily variation in IWV [13], inhomogeneities during the passage of fronts [14, 15]. The coherence of mesoscale variations in precipitation intensity and convective available potential energy with variations in ZTD of GNSS signals was discovered in [16]. In [17], a regression model of the relationship between IWV, the intensity of extreme precipitation, and the convective available potential energy was developed.

This work identifies differences in atmospheric characteristics during a period of deep convection above the antenna of a satellite signal detector by assessing fluctuations in the horizontal gradient parameters of ZTD depending on the convection indices, which are used to forecast hazardous meteorological phenomena.

The zonal and meridional horizontal gradient parameters of ZTD (ZTD gradient vector components) are converted to the gradient value dZTD and the gradient direction $A_{d\mathrm{ZTD}}$:

$$d\mathrm{ZTD} = \sqrt{{}^n\mathrm{ZTD}^2 + {}^e\mathrm{ZTD}^2}, \quad A_{d\mathrm{ZTD}} = \arctan\left(\frac{{}^n\mathrm{ZTD}}{{}^e\mathrm{ZTD}}\right). \quad (3)$$

Long series of dZTD and $A_{d\mathrm{ZTD}}$ with a time resolution of 5 min have been calculated based of data from the network of stations in Kazan and the Republic of Tatarstan over 2013–2021. Standard deviations of daily variations in dZTD and $A_{d\mathrm{ZTD}}$ are estimated as characteristics of the intensity of mesoscale variations in the troposphere.

Based on the ERA5 reanalysis data derived with the model of the European Center for Weather Forecasting ECMWF [18], physical and statistical parameters of instability have been calculated. Convection indices are commonly used both to assess the probability of hazardous events and to test the success of their forecast [19–27].

To assess the probability of hazardous phenomena due to convection, complex indices have been selected from a variety of parameters, which are often used for estimation of the risk of tornadoes, showers, and thunderstorms [19, 22, 25].

Upward vertical velocity (UVV) [24]:

$$\mathrm{UVV} = \sqrt{2\mathrm{CAPE}},$$

where CAPE (convective available potential energy) represents the work an air particle can do during adiabatic ascent [18]:

$$\mathrm{CAPE} = g\int_{z_{\mathrm{base}}}^{z_{\mathrm{top}}} \frac{T_{\mathrm{p}} - T_{\mathrm{v}}}{T_{\mathrm{v}}}.$$

Here, T_{v} and T_{p} are the virtual temperatures of the medium and the ascending particle; g is the acceleration of gravity; z_{base} is the height of the most unstable layer below the level 350 hPa; z_{top} is the height of the model level where the vertical speed decreases to zero. The CAPE is calculated under the assumption that air particles do not mix with the surrounding air; the ascent is pseudoadiabatic [28].

The upward flow is considered strong if UVV = 40 m/s and very strong at UVV = 60 m/s. The probability of large hail increases with UVV [21].

The vortex generation parameter (VGP) is an indirect measure of the tilt of the horizontal vortex. It is defined as [23]:

$$\mathrm{VGP} = \sqrt{2\mathrm{CAPE}}\,\mathrm{MLS},$$

where MLS (mid-level shear) is the wind shear in a 3 km layer. The strong shear in this layer contributes to high helicity: the higher the MLS, the longer the convection.

Table 1. Median IWV and *d*ZTD and its fluctuations for samples corresponding to the boundary values of convection indices (strong and weak convection according to a convection index)

Parameter	UVV		VGP		WMAXSHEAR	
	≥40 m/s	<40 m/s	≥400 m^2/s^2	<400 m^2/s^2	≥400 m^2/s^2	<400 m^2/s^2
IWV, mm	35	23	35	23	33	23
*d*ZTD, mm	0.87	0.73	0.89	0.73	0.87	0.72
Daily fluctuations of *d*ZTD, mm	0.45	0.37	0.46	0.36	0.47	0.36
Daily fluctuations of $A_{d\mathrm{ZTD}}$	27	21	26	21	26	21

The complex WMAXSHEAR index also indicates a deep convection and takes into account both vertical flow and wind shear in a 6 km layer [25]:

$$\mathrm{WMAXSHEAR} = \sqrt{2\mathrm{CAPE}}\,\mathrm{DLS},$$

DLS is the deep layer shear.

The UVV, VGP, and WMAXSHEAR indices were calculated from ERA5 data for the coordinates of GNSS receiver antennas in the Republic of Tatarstan. Since the spatial resolution of ERA5 is 0.25°, two-dimensional linear interpolation was used to found these parameters at a GNSS receiver point.

RESULTS AND DISCUSSION

Long series (2013–2021) of all convective indices under study were calculated with a time step of 1 h. Samples of *d*ZTD and $A_{d\mathrm{ZTD}}$ have been compiled for each of the parameters according to their critical values, which characterize the conditions of weak and strong convection. The samples have been compiled only for conventional observation periods from April 15 to September 15. Then, we have pairwise compared the distributions of the samples of ZTD gradient parameters for each index.

The Pearson test shows that the distributions of the horizontal gradient parameters of ZTD are not normal. Therefore, for pairwise check of the differences in the distributions corresponding to strong and weak convections, not only Student's tests and ANOVA, but also the Kruskal–Wallis test (testing for equality of median sample values) are used. The distributions of the parameters of the horizontal ZTD gradient have been found to be significantly different under conditions of strong and weak convection according to all statistical criteria.

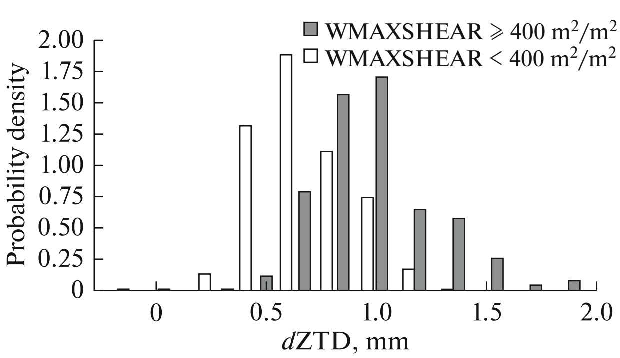

Fig. 1. Distribution of *d*ZTD samples for weak and strong convection conditions according to the WMAXSHEAR index.

Table 1 presents the boundary values of the convection indices used in the study for sampling GNSS monitoring data and the corresponding medians of IWV, gradient value, and gradient fluctuations under conditions of strong and weak convection.

In [29], we showed that IWV calculated from GNSS monitoring data in the Volga region significantly changes its distribution in summer under conditions of deep convection, its median increases by 12 mm on average.

Over the period under study, the coefficient of correlation between UVV, VGP, and WMAXSHEAR indices is 0.86–0.95. It is expected that the atmospheric fields of IWV and ZTD of GNSS signals discriminated by various convection indices have similar characteristics.

One can seen an increase in IWV by more than 10 mm of precipitable water under conditions of strong convection. Convective processes produce mesoscale inhomogeneities, which contributes to the increase in *d*ZTD by 20% and in its standard deviation by 25%. Fluctuations of ZTD gradient direction of GNSS radio signals also increase.

Figures 1–3 show example of empirical distributions of samples of the amplitude, value, and direction of the ZTD gradient parameter derived from discrimination by convection indices.

Like statistical criteria, these figures show that atmospheric parameters derived from GNSS sounding data significantly change under conditions of deep convection. The correlation with the daily maxima of the convection indices in summer and the daily average values of IWV is maximal for the VGP index and is equal to 0.6. The same index showed the strongest correlation (0.4) with $A_{d\mathrm{ZTD}}$ fluctuations. Such correlation coefficients are characteristic of a significant but nonlinear relationship between parameters.

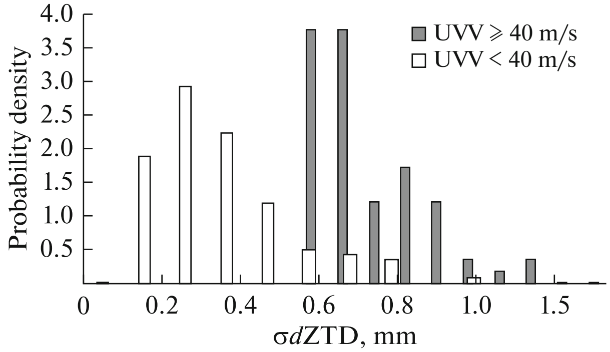

Fig. 2. Distribution of the samples of the standard deviation of *d*ZTD for weak and strong convection conditions according to the UVV index.

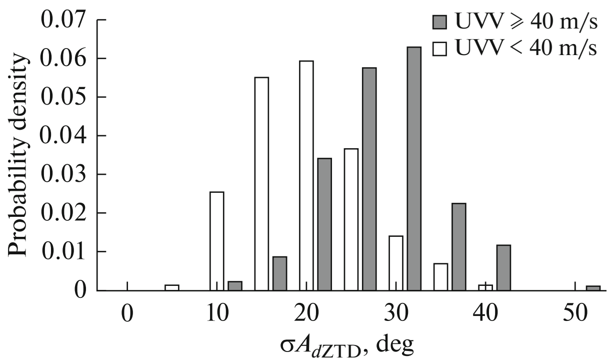

Fig. 3. Same as in Fig. 2, but for A_{dZTD}.

Selection of summer days by IWV has shown that the use of fluctuations of gradient parameters as additional sampling criteria increases the value of convection indices on these days. For example, if IWV is set equal to 25 mm of precipitable water, then the UVV median is 27 m/s at Kazan. If we remove days with fluctuations of ZTD gradient angle less than 20° from a sample, then the median UVV increases to 30 m/s, whereas it is equal to 10 m/s in the summers under study. However, the task of determining criteria for assessing the intensity of convective processes based on GNSS data requires additional research. Work [10], where an attempt was made to develop such a criterion, was not further developed for unknown reasons. Additional consideration of real-time gradient parameters was used to study the possibility of thunderstorm forecasting in Bulgaria [30].

CONCLUSIONS

Our research confirms that the use of global navigation satellite systems for remote sensing of the troposphere is an effective tool for satellite monitoring of convective processes. The rapid development of atmospheric inhomogeneities, which can signal the development of hazardous weather phenomena, such as heavy precipitation, thunderstorms, and tornadoes, manifests itself in IWV and the gradient parameters of ZTD of GNSS radio signals. This means a possibility of rapidly receiving data on the state of the atmosphere with a high time resolution and responding to possible hazards.

FUNDING

The study was supported by the Russian Science Foundation (grant no. 23-27-00222) (https://rscf.ru/project/23-27-00222) (project no. 23-27-00222). GNSS monitoring data was collected with the support of the strategic academic leadership program of the Kazan (Volga region) Federal University (“PRIORITY-2030”).

CONFLICT OF INTEREST

The authors of this work declare that they have no conflicts of interest.

REFERENCES

1. A. V. Chernokulsky, A. V. Eliseev, F. A. Kozlov, N. N. Korshunova, M. V. Kurgansky, I. I. Mokhov, V. A. Semenov, N. V. Shvets’, A. N. Shikhov, and Yu. I. Yarinich, “atmOspheric severe convective events in Russia: Changes observed from different data,” Rus. Meteorol. Hydrol. **47** (5), 343–354 (2022).
2. A. N. Shikhov, A. V. Chernokulsky, A. A. Sprygin, and Yu. I. Yarinich, “Estimation of convective atmospheric instability during squalls, tornadoes, and large hail events from satellite observations and ERA5 reanalysis data,” Atmos. Ocean. Opt. **35** (6), 793–801 (2022).
3. A. O. Semenov, Ya. A. Virolainen, Yu. M. Timofeev, and A. V. Poberovskii, “Comparison of ground-based FTIR and radio sounding measurements of water vapor total content,” Atmos. Ocean. Opt. **28** (2), 121–125 (2015).
4. R. Santerre, *GPS Satellite Sky Distribution: Impact on the Propagation of Some Important Errors in Precise Relative Positioning* (UNB, Brunswick, 1989).
5. M. S. Bevis and T. A. Businger, “GPS meteorology: Remote sensing of atmospheric water vapor using the global positioning system,” J. Geophys. Res. **97** (D14), 15787–15801 (1992).
6. Y. E. Bar-Sever, P. M. Kroger, and J. A. Borjesson, “Estimating horizontal gradients of tropospheric path delay with a single GPS receiver,” JGR **103** (B3), 5019–5035 (1998).
7. G. Elgered, T. Ning, P. Forkman, and R. Haas, “On the information content in linear horizontal delay gradients estimated from space geodesy observations,” Atmos. Meas. Tech. **12**, 3805–3823 (2019).
8. X. Li, F. Zus, C. Lu, T. Ning, G. Dick, M. Ge, J. Wickert, and H. Schuh, “Retrieving high-resolution tropospheric gradients from multiconstellation GNSS observations,” Geophys. Rev. Lett. **42**, 4173–4181 (2015).
9. S. Barindelli, E. Realini, G. Venuti, A. Fermi, and A. Gatti, “Detection of water vapor time variations as-

sociated with heavy rain in northern Italy by geodetic and low-cost GNSS receivers," Earth Planets Space **70** (1), 1–18 (2018).

10. H. Brenot, J. Nemeghaire, L. Delobbe, N. Clerbaux, P. De Meutter, A. Deckmyn, A. Delcloo, L. Frappez, and M. Van Roozendael, "Preliminary signs of the initiation of deep convection by GNSS," Atmos. Chem. Phys. **13**, 5425–5449 (2013).
11. G. Nykiel, M. Figurski, and Z. Baldysz, "Analysis of GNSS sensed precipitable water vapour and tropospheric gradients during the derecho event in Poland of 11th August 2017," J. Atmos. Sol.-Terr. Phys. **193**, 105082 (2019).
12. V. Graffigna, M. Hernandez Pajares, F. Azpilicueta, and M. Gende, "Comprehensive study on the tropospheric wet delay and horizontal gradients during a severe weather event," Remote Sens. **14** (4), 888 (2022).
13. V. V. Kalinnikov and O. G. Khutorova, "Diurnal variations in integrated water vapor derived from a GPS ground network in the Volga-Ural region of Russia," Ann. Geophys. **35**, 453–464 (2017).
14. O. G. Khutorova, V. E. Khutorov, V. V. Dement'ev, A. S. Blizorukov, and G. E. Korchagin, "Variability of Atmospheric Moisture Fields from GPS-GLONASS sounding data near Kazan," Sovremennye Problemy Distantsionnogo Zondirovaniya Zemli Kosmosa **15** (3), 252–260 (2018).
15. M. F. Camisaya, J. A. Rivera, M. L. Mateo, P. V. Morihetti, and M. V. Mackern, "Estimation of integrated water vapor derived from global navigation satellite system observations over central-western Argentina (2015–2018). Validation and usefulness for the understanding of regional precipitation events," J. Atmos. Sol.-Terr. Phys. **197**, 1–12 (2020).
16. O. G. Khutorova, M. V. Maslova, and V. E. Khutorov, "Monitoring of convective processes with satellite navigation system receivers," Opt. Atmos. Okeana **35** (6), 505–509 (2022). https://doi.org/10.15372/AOO20220612
17. M. R. Ziarani, B. Bookhagen, T. Schmidt, J. Wickert, A. De la Torre, Z. Deng, and A. A. Calori, "Model for the relationship between rainfall, GNSS-derived integrated water vapour, and CAPE in the Eastern Central Andes," Remote Sens. **13** (18), 1–19 (2021).
18. H. Hersbach, B. Bell, P. Berrisford, S. Hirahara, A. Horanyi, J. Munoz-Sabater, J. Nicolas, C. Peubey, R. Radu, D. Schepers, A. Simmons, C. Soci, S. Abdalla, X. Abellan, G. Balsamo, P. Bechtold, G. Biavati, J. Bidlot, M. Bonavita, G. De Chiara, P. Dahlgren, D. Dee, M. Diamantakis, R. Dragani, J. Flemming, R. Forbes, M. Fuentes, A. Geer, L. Haimberger, S. Healy, R. J. Hogan, E. Holm, M. Janiskova, S. Keeley, P. Laloyaux, P. Lopez, C. Lupu, G. Radnoti, P. Rosnay de, I. Rozum, F. Vamborg, S. Villaume, and J.-N. Thepaut, "The ERA5 global reanalysis," Q.J.R. Meteorol. Soc. **146** (730), 1999–2049 (2020).
19. D. O. Blanchard, "Assessing the vertical distribution of convective available potential energy," Weather Forecast **13** (3), 870–877 (1998).
20. H. B. Brooks, C. A. Doswell, and R. B. Wilhelmson, "The role of midtropospheric winds in the evolution and maintenance of low-level mesocyclones," Mon. Weather. Rev. **122**, 126–136 (1994).
21. D. W. Burgess and L. R. Lemon, "Severe thunderstorm detection by radar," Radar Meteorol. Am. Meteorol. Soc., 619–647 (1990).
22. R. C. Miller, *Notes on analysis and severe storm forecasting procedures of the Air Force Global Weather Center. Tech. Report No. 200* (Scott AFB, Illinois, 1972).
23. E. N. Rasmussen and D. O. Blanchard, "A baseline climatology of sounding-derived supercell and tornado forecast parameters," Weather Forecast **13** (13), 1148–1164 (1998).
24. J. Gracier, Convection parameters. http://www.juergen-griser.de/Convection Parameters/ConvectionParameters.pdf. Cited June 20, 2023.
25. M. Taszarek, H. E. Brooks, and B. Czernecki, "Sounding-derived parameters associated with convective hazards in Europe," Mon. Weather. Rev. **145** (4), 1511–1528 (2017).
26. D. Jelic, M. T. Prtenjak, B. Malecic, A. B. Vozila, O. A. Megyeri, and T. Renko, "A new approach for the analysis of deep convective events: Thunderstorm intensity index," Atmosphere **12** (7), 908–934 (2021).
27. I. M. Gubenko and K. G. Rubinshtein, "Analysis of comprehensive forecast of lightning activity," Opt. Atmos. Okeana **33** (12), 949–957 (2020). https://doi.org/10.15372/AOO20201208
28. www.ecmwf.int/en/elibrary/81271-ifs-documentation-cy47r3-part-iv-physical-processes. Cited June 20, 2023.
29. O. G. Khutorova, M. V. Maslova, and V. E. Khutorov, "Manifestation of convective processes in series of integrated water vapor compiled based on long-term GPS monitoring of the troposphere in Kazan," Sovremennye Problemy Distantsionnogo Zondirovaniya Zemli Kosmosa **20** (3), 271–281 (2023).
30. G. Guerova, J. Dousa, T. Dimitrova, A. Stoycheva, P. Vaclavovic, and N. Penov, "GNSS storm nowcasting demonstrator for Bulgaria," Remote Sens. **14** (15), 3746 (2022).

Publisher's Note. Pleiades Publishing remains neutral with regard to jurisdictional claims in published maps and institutional affiliations.